Polymer Chemistry

Accepted Manuscript

ROYAL SOCIETY OF CHEMISTRY

www.rsc.org/polymers

Cite this: DOI: 10.1039/c0xx00000x

www.rsc.org/xxxxxx

PAPER

Crystallization-promoted emission enhancement of poly(L-lactide) containing a fluorescent salicylideneazine center with aggregation-enhanced emission property

Tai-Shen Hsiao, Po-Chiao Huang, Li-Yang Lin, Deng-Jie Yang, Jin-Long Hong*

Received (in XXX, XXX) Xth XXXXXXXXX 20XX, Accepted Xth XXXXXXXXX 20XX
DOI: 10.1039/b000000x

Fluorescent 1,2-bis(2,4-dicydroxybenzylidene)hydrazine (CN4OH) with aggregation-enhanced emission (AEE) property was used as initiator to induce ring-opening polymerization (ROP) of L-lactide, resulting in polymer CN-PLLA(n)s containing an AEE-active CN center. With both pairs of *p*- and *o*-hydroxyl (OH) groups, CN4OH initiates ROP of L-lactide solely by the *p*-OH groups and the resulting CN-PLLA(n)s are highly-emissive due to the rotational restriction imposed by the remaining *p*-OHs of the central CN unit. Study on the solid emission of CN-PLLA(n)s reveals that crystallization of the neighbouring PLLA chains, instead of the fluorescent CN center itself, determines the AEE activity, e.g. emission of the crystalline CN-PLLA(n)s is much higher in emission intensity than the amorphous CN-PLLA(n)s. As restricted molecular rotation is the main mechanism leading to the AEE activity, effective rotational restriction imposed by the crystalline polylactide chains is responsible for the high emission of the crystalline CN-PLLA(n)s, in contrast to the weak emission of the amorphous CN-PLLAs. The emission promotion of the fluorescent CN center by the neighbouring polylacide chains is designated as crystallization-promoted emission enhancement (CPEE) and is the focus of the study.

Introduction

In 2001, Tang's group[1,2] discovered that the propeller-shaped molecule of 1-methyl-1,2,3,4,5-pentaphenylsilole (MPPS) emits strongly in the aggregated solution and solid film states despite it is non-emissive in dilute solution. This concentration-dependent emission behaviour was designated as aggregation-induced emission (AIE). With beneficial emission efficiency in the solid film state, lots of organic and polymeric fluorophores with AIE or aggregation-enhance emission (AEE) properties[3-8] have been prepared and characterized. Although an AIE process may mechanistically be associated with pathways like J-aggregate formation (JAF),[9] twisted intramolecular charge transfer (TICT),[10-12] and excited-state intramolecular proton transfer (ESIPT),[13] the intrinsic mechanism is actually due to the effective restriction on the intramolecular motions of the AIE-active fluorophores. Study[14] on AIE-active fluorophores of different molecular shapes has concluded that the restriction of intramolecular rotations and vibrations (RIR and RIV) are the main causes for the AIE phenomena observed in the propeller-shaped and shell-like fluorophores, respectively. Similar to the first discovered silole derivative of MPPS,[1,2] most of the AIE-active fluorophores are propeller-like molecules. In the aggregated state of MPPS, the sluggish molecular rotation[15,16] of the aromatic rings reduces the possibilities of non-radiative decay pathways and results in the enhanced emission.

Crystallization is an important factor contributing to the intense solid state's emission in view that fluorophores with crystallization-enhanced emission (CEE)[17-22] properties are highly-emissive in the solid crystalline state but are weakly emissive when they are in the amorphous aggregated state. It is considered that amorphous aggregates consist of more molecular voids and free volumes allow free molecular rotation but in the crystalline phase, fluorescent molecules are fastened by the intimately-packed crystalline lattice and rotational restriction imposed by the crystalline lattice are so efficient that the crystalline fluorophores are no longer free to rotate, thus, deactivating the non-radiative decay pathway to result in high emission with intensity much higher than the amorphous counterparts. The interesting CEE property also exists in blend systems. For example, AEE-active blends of bis(pyridinylvinyl)anthracene (An2Py)[23] and bisphenol A (BPA), with good miscibility due to the facile hydrogen bond (H bonded) interactions between pyridinyl rings of An2Py and hydroxyl (OH) groups of BPA, show strong emission due to the CEE property. Wide-angle X-ray diffraction (WAXD) spectra indicate that incorporation of BPA generates new crystal, within which effective rotational restriction on the An2Py molecules results in blends emitting with higher intensity than the pure An2Py itself.

Polylactide of formula (-[$CH(CH_3)COO]_n$-), as the polyester equivalent of the polypeptide polyalanine (-[$CH(CH_3)CONH]_n$, is a biodegradable crystalline polymer produced from renewable biomass such as sugar, and it exhibits the biocompatibility and high mechanical performances comparable to those of petroleum-based traditional polymers.[24] Since a heteroatom is present in the main chain (which has a chemical polarity), it is a

genuine chiral polymer, the two enantiomers of which have been synthesized. Optical purity of the monomer has a great deal to do with the structure-property relationship of PLA. For example, pure isotactic poly(L-lactic acid) (PLLA) are semicrystalline; nevertheless, poly(D,L-lactic acid) (PDLLA) is amorphous. Pure PLLA is known to form three kinds of crystal modifications (α, β and γ forms)[25-29] with versatile crystal structures and polymorphism[30-32] dependent on preparation methods and thermal history. Synthetically, high MW PLLA can be easily prepared from ring-opening polymerization of L-lactide monomer[33] in the presence of OH-containing initiator and tin catalyst.

The AIE-active fluorophore of 1,2-bis(2,4-dihydroxybenzylidene)hydrazine[34] (CN4OH, Scheme 1) is an interesting fluorophore with its emission behaviour strongly associated with ESIPT[13,35-41] of the inherent enolimine rings bridged by intramolecular H bond interactions. Upon photoexcitation, fast transfer of hydroxyl proton to imine nitrogen quickly converts the excited enol (E*) into the excited keto (K*) responsible for the emission. When in the solution state, CN4OH[34] emits weakly due to the non-radiative decay of the twisted ketonic excited state but in the aggregated state, a planar dimer structure containing rigid enolimine rings is responsible for the observed intense emission. Intramolecular H bond interactions between the *o*-OHs and the imine nitrogen lead to effective RIR and the intense fluorescence. With no *o*-OH groups to impose the required rotational restriction, 1,2-dibenzylidenehydrazine (DB, Scheme 1) is non-emissive. Previously, we had prepared homogeneous blends of CN4OH and poly(vinylpyridine) (PVP)[42] through preferable intermolecular H-bond interactions between the pyridinyl rings of PVP and the *p*-OHs of CN4OH. When the applied pyridinyl rings of PVP are less than the equivalent amounts of the *p*-OH groups of CN4OH, the resulting blends exhibited enhanced emission and the accompanied increase of the blends' crystallinity; however, when more than equivalent amounts of PVP were applied in the blends, excess pyridinyl rings of PVP started to H-bond to the *o*-OHs of CN4OH, destructing the crystalline packing of the blends to reduce the emission intensity. The results clearly suggest that the labile *p*-OHs, in contrast to the inert *o*-OHs stabilized by intramolecular H-bonds, of CN4OH are the primary reactive sites responsive to external additives.

In this study, the reactive *p*-OHs of CN4OH were used as initiating sites to induce ring-opening polymerization (ROP, Scheme 1) of L-lactide, affording crystalline CN-PLLA(n)s of different MWs. In contrast, the *o*-OHs of CN4OH survived after ROP and served as H bonding sites to maintain the rigid enolimine rings of the CN center in the resulting CN-PLLA(n)s. The rigid enilimine rings of the CN center are clumsy in rotation and therefore, induce AEE activity of CN-PLLA(n)s. Further study suggested that emission efficiency of CN-PLLA(n)s is strongly correlated with the crystallinity of the surrounding PLLA chains. Instead of the fluorescent CN itself, the crystallinity of the non-fluorescent PLLA promotes the emission efficiency of the crystalline CN-PLLA(n), this crystallization-promoted emission enhancement (CPEE) can be best illustrated by Scheme 2 that the amorphous CN-PLLA(n)s are weak emitters while crystalline CN-PLLA(n)s are much higher in emission intensity than the amorphous CN-PLLA(n)s. The CPEE property is attributed to the relative rotational restriction that the crystalline and the amorphous PLLA chains impose on the central CN unit. To address the effect of rotational restriction, CN-PLLA(n)s with different MWs and crystallinities were prepared and their solution and solid emission behaviours are evaluated in an effort to reveal the relationship between crystallinity, rotational restriction and CPEE-related emission behaviour.

Experimental

Materials

L-lactide (Alfa Aesar, 98 %) and tin(II) 2-ethylhexanoate ($Sn(Oct)_2$, Alfa Aesar, 96%) were used directly without purification. Tetrahydrofuran (THF) was refluxed over mixtures of sodium/benzophenone whereas N,N-dimethylforamide (DMF) and toluene were refluxed over CaH_2 for 5 h in prior to distillations for use. CN4OH and CN2OH were prepared according to previous procedures.[42]

Preparation of CN-PLLA(n)s:

The CN-PLLA(n)s were prepared by ROP of L-lactide initiated by (CN4OH). The preparation procedures illustrated in Scheme 1 were detailed below.

The preparation of low MW CN-PLLA(10) oligomer was given as the representative example. In a 25 ml pre-dried round-bottomed flask, a reaction mixture of L-lactide (78 mg, 0.54 mmol) and CN4OH (4 mg, 0.0147 mmol) in dry THF (5 ml) was stirred for 10 min before the injection of $Sn(Oct)_2$ (5 mml, 12.5 mmol) catalyst. The reaction mixtures (molar ratio of L-lactide/CN4OH/$Sn(Oct)_2$ = 37/1/1) were stirred at room temperature for 6 h before precipitation of the crude product from hexane. The precipitant was then washed with hexane once and isopropanol twice. The resulting solid was then filtered, dried in vacuum to obtain the final product of CN-PLLA(10). Recipes of lactide/CN4OH/$Sn(Oct)_2$ = 100/1/1 and 350/1/1 were used in the preparation of high MW CN-PLLA(21) and CN-PLLA(145), respectively, and reactions were performed in a mixture solvent of DMF/toluene (v/v = 1/10) at reflux temperature. The resulting products were under the same purification procedure used in CN-PLLA(10). ^{1}H NMR (500 MHz, d_6-DMSO); CN-PLLA(10): • 11.3 (s, 2H, H_a), 8.76 (s, 2H, H_b), 6.61 (d, 2H, H_c), 6.4 (d, 2H, H_d), 6.31 (d, 2H, H_e), 5.43 (q, H, H_f), 5.2 (q, H, H_g), 1.44 (d, 3H, H_h), 1.4 (d, 3H, H_i) (Figure S1); CN-PLLA(21): δ 5.43 (q, H, H_a), 4.25 (q, H, H_b), 1.44 (d, 3H, H_c), 1.4 (d, 3H, H_d) (Figure S3); CN-PLLA(145): δ 5.18 (broad, H, H_a), 4.37 (broad, H, H_b), 1.6 (broad, 3H, H_c), 1.31 (broad, 3H, H_d) (Figure S5). ^{13}C NMR (500 MHz, d_6-DMSO); CN-PLLA(21): δ 16.4 (C_d), 20.7 (C_c), 66.0 (C_b), 69.1 (C_a) 170.0 (C_g), 170.6 (C_h), 172.1 (C_j), 172.6 (C_f), 175.0 (C_e), 177.2 (C_i), 177.4 (C_k) (Figure S8); CN-PLLA(145): δ16.4 (C_d), 20.7 (C_c), 66.8 (C_b), 69.3 (C_a), 170.4(C_g), 171.1(C_h), 174.2 (C_j), 174.4 (C_f), 176.0 (C_e), 179.0 (C_i), 179.2(C_k) (Figure S9). FTIR (KBr pellet, cm^{-1}); CN-PLLA(21): 2997, 2944, 1759, 1633, 1454, 1208, 1362, 1125, 1042. CN-PLLA(145): 2999, 2944, 1755, 1633, 1461, 1208, 1373, 1137, 1044 (Figure S10). MALDI-TOF (Dalton): CN-PLLA(10), M_n = 1,026, M_w = 1,041, PDI = 1.01 (Figure S2); CN-PLLA(21), M_n = 1,833, M_w = 1,871, PDI = 1.02 (Figure S4); CN-PLLA(145), M_n = 10,750, M_w = 12,362, PDI = 1.15 (Figure S6).

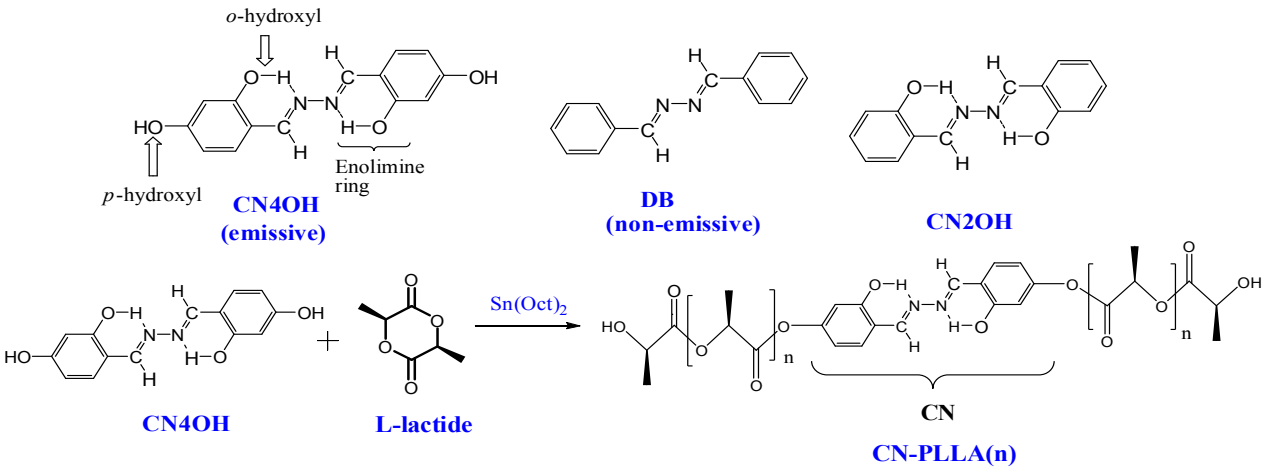

Scheme 1 Chemical structure of CN4OH and DB and ring-open polymerization of L-lactide initiated by the *o*-OH groups of CN4OH to generate CN-PLLA(n)s.

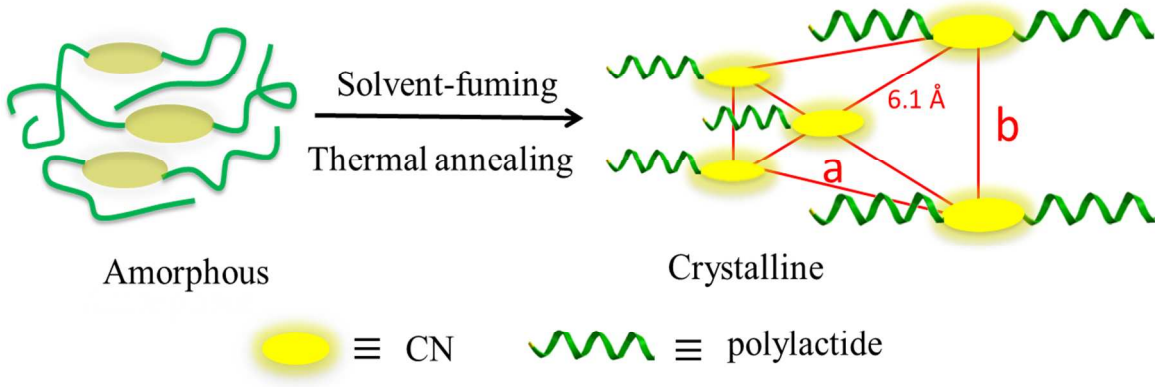

Scheme 2 Transformation of chain conformation from amorphous to crystalline states.

Characterization

^{1}H NMR spectra were recorded with a Varian VXR-500 MHz FT-NMR instrument with tetramethylsilane (TMS) as internal standard. The emission spectra were obtained from a LabGuide X350 fluorescence spectrophotometer using a 450 W Xe lamp as the continuous light source. A quartz cell with dimensions of 0.2 x 1.0 x 4.5 cm^3 was used for the solution samples. Stock solutions of the organic and polymeric fluorophores with a concentration of 10^{-3} M in THF were first prepared. Aliquots of these stock solutions were transferred to 10 mL volumetric flasks, into which appropriate volumes of THF and water were added dropwise under vigorous stirring to furnish 10^{-4} M solutions with a water content ranged from 0 to 90 v%. Solid samples were prepared by drop-casting sample solutions over quartz plates. For solvent-fuming treatment, the sample plates were placed in a close channel saturated with ethanol vapor. Quantum yield (Φ_F) of the solution sample was determined by using a quinine sulfate standard solution. An integrating sphere was used for the solid sample. A wide-angle X-ray diffraction (WAXD) pattern was obtained from a Siemens D5000 X-ray diffractometer with a source of Cu Kα (l¼ 0.154 nm) radiation at 40 kV and 30 mA. Diffraction patterns were collected with a scan rate of 3 s per 0.1 °. The WAXD spectra were resolved by curve-fitting into crystalline and amorphous background regions (Figure S14, supporting information). The ratio of the integrated diffraction intensity of the crystalline peak to the whole scattering was then evaluated as crystallinity. Mass spectra were recorded using a Bruker Daltonics Autoflex MALDI-TOF mass spectrometer. Particle sizes of the aggregates in solutions were measured by dynamic light scattering (DLS) using a Brookhaven 90 plus spectrometer equipped with a temperature controller. An argon ion laser operating at 658 nm was used as the light source. Thermal transition of polymer was determined from a TA Q-20

differential scanning calorimeter (DSC) calorimeter with a scan rate of 10 °C/min under nitrogen.

Results and discussion

As illustrated in Scheme 1, the target polymer CN-PLLA(n)s were prepared by ROP of L-lactide initiated by CN4OH in the presence of $Sn(Oct)_2$ catalyst. Appropriate employments of monomer/initiator ratio, reaction temperature and solvent, three CN-PLLA(n)s with MW ranged from 10^3 to 10^4 Dalton (Table 1) can be readily prepared. Of the three polymer products, the low MW oligomer CN-PLLA(10) is used as spectral standard to identify the unique role of *p*-OH groups as the initiating sites for ROP. The *o*-OHs of CN4OH remained intact during ROP and functions as H bonding sites to maintain the rigid enolimine rings required for the high emission of the resulting CN-PLLA(n)s. Spectral identification of CN-PLLA(10) was therefore conducted in prior to the emission characterization of CN-PLLA(21) and (145).

Molecule of CN2OH (cf. Scheme 1) with the sole *o*-OH groups was particularly synthesized and compared with CN4OH on the ^{1}H NMR spectra. Figure 1 summarizes the solution ^{1}H NMR spectra of CN2OH, CN4OH, mixtures of CN4OH/$Sn(Oct)_2$ and the oligomeric CN-PLLA(10). To have unambiguous spectral interpretation, all spectra were measured on solutions with constant fluorophore's concentration (= 10^{-3} M). The *o*-OH protons (**a** and **a'**) of CN2OH and CN4OH resonance in close vicinities of 11.12 and 11.38 ppm, respectively; therefore, the resonance peak at an upper field of 10.18 ppm should be attributed to the *p*-OH protons (**b'**) of CN4OH. The preferable binding of the *p*-OH groups to $Sn(Oct)_2$ catalyst, as the primary step leading to ROP of L-lactide, can then be verified by the spectra of CN4OH/$Sn(Oct)_2$ mixtures. Primarily, complexation causes large reduction on the resonance peak of *p*-OH protons (at 10.18 ppm) in the spectrum of CN4OH/$Sn(Oct)_2$(1/1). Meanwhile, we observed the emergence of a broad resonance (c*) peak at 11.97 ppm. This broad resonance peak is due to the tin-incorporated *p*-OH protons and it becomes broader and larger in intensity, with the concurrent intensity reduction of the resonance peak of the *p*-OH protons at 10.18 ppm, in the spectrum of the CN4OH/$Sn(Oct)_2$(1/2) containing large amounts of $Sn(Oct)_2$. It was previously reported that this broad "alcoholic proton" resonance[43] is due to the resonance of the combined ROH and octanoic acid protons, which undergo rapid exchange relative to the NMR time scale. Therefore, the alcoholic protons (c*) in the spectrum of CN4OH/$Sn(Oct)_2$(1/1) is mainly from the reaction of *p*-OH protons to tin catalyst but for the CN4OH/$Sn(Oct)_2$(1/2) solution with excess $Sn(Oct)_2$, certain fractions of *o*-OH groups will bind to $Sn(Oct)_2$, resulting in the intensity reduction of the peak at 11.38 ppm. To preserve the *o*-OH groups of CN4OH, the polymerization needs to be operated under the condition that the molar ratio of $Sn(Oct)_2$/CN4OH is kept at one.

With discernible signals of the OH protons, low MW CN-PLLA(10) oligomer was prepared to confirm that the *o*-OH groups of CN4OH can be kept intact without participating in ROP. The corresponding ^{1}H NMR spectrum in Figure 1 clearly contains the resonance peak of *o*-OH protons (**a''**) at 11.38 ppm; meanwhile, absence of resonance peak at 10.18 ppm indicates that all the *p*-OH groups should already be consumed by the lactide monomers during ROP. Although visible, all OHs and aromatic resonance peaks of CN-PLLA(10) are much lower in intensity than other spectra in Figure 1, which is associated with the restricted molecular rotation of the CN unit.

Previously, the ^{1}H NMR spectra were used for the detection of the rotation-induced conformational changes on the AIE-active silole derivative.[15,16] The analysis is based on the principle that the fast conformational exchanges caused by the fast molecular rotations give sharp resonance peaks, whereas the slower exchanges due to restricted molecular rotation broaden the resonance peaks. The ^{1}H NMR analysis was then extended to polymer[44] and polymer blend[45] systems and the results suggest that the rotational restrictions in these systems are so effective that the corresponding resonance bands became reduced in intensity or disappeared due to the insufficient power of the magnetic field in igniting the molecular motion of the frozen bonds. With respect to evaluate the possible rotational restriction imposed by the polymeric PLLA chains, solution spectrum of oligomeric CN-PLLA(10) with discernible aromatic resonance peaks was compared with the spectrum of CN4OH in Figure 2.

The solution spectra in Figure 2 were operated at a constant concentration (10^{-3} M) of the fluorescent unit; therefore, we would expect aromatic resonance peaks in both spectra should be the same if no other controlling factor came into play. For CN4OH, the aromatic protons a, b and c contribute to the split resonance peaks at 7.42, 6.39 and 6.32 ppm, respectively. The corresponding aromatic resonance peaks are still resolvable in the spectrum of CN-PLLA(10); however, they became smaller in intensity than those of CN4OH despite both spectra were conducted with the same fluorophore's concentration (10^{-3} M). In the dilute solution state, the inherent PLLA chains function to hamper the rotation of the single bonds linking to the CN center, making the conformation change of the central aromatic rings difficult to be detected by the ^{1}H NMR. From the spectra of CN4OH to CN-PLLA(10), the peak intensities of the aromatic resonances were significant decreased, the beneficial role of PLLA chains as rotation blocker is herein certified. Compared to short PLLA chains in the oligomeric CN-PLLA(10), the long chains of CN-PLLA(21) and (145) are supposed to be more effective in hampering the rotational motions of the CN centers in view of the large dragging forces of the long polymer chains. We would expect more emission enhancement of the CN-PLLA(21) and (145) solutions when compared to the oligomeric CN-PLLA(10).

Table 1 MWs of CN-PLLAs evaluated from MALDI-TOF mass spectroscopy.

Polymer	From MALDI-TOF
CN-PLLA(145)	M_n = 10750 (n = 145), M_w = 12362, PDI = 1.15
CN-PLLA(21)	M_n = 1833 (n = 21), M_w = 1871, PDI = 1.02
CN-PLLA(10)	M_n = 1026 (n = 10), M_w = 1041, PDI = 1.01

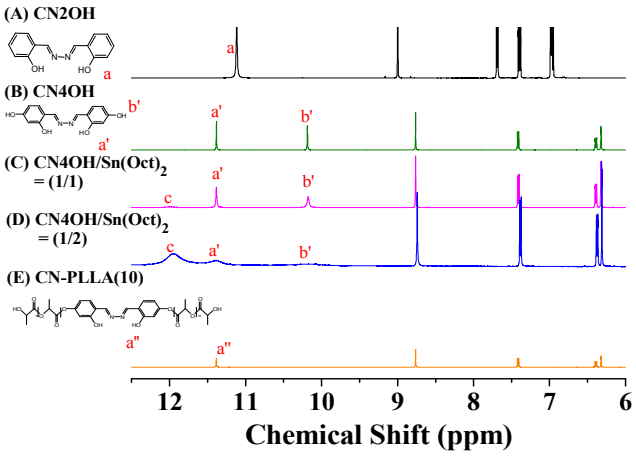

Figure 1 ^{1}H NMR of (A) CN2OH, (B) CN4OH, (C) CN4OH/Sn(Oct)$_2$(1/1) and (D) CN4OH/Sn(Oct)$_2$(1/2) and (E) CN-PLLA(10) (in d_6-DMSO).

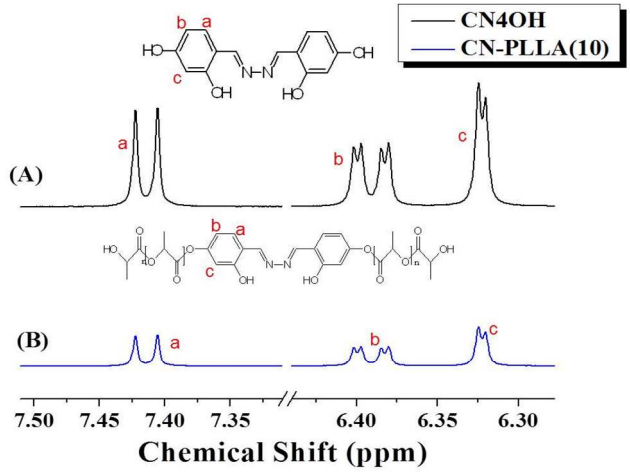

Figure 2 ^{1}H NMR of (A) CN4OH (= 10^{-3} M) and (B) CN-PLLA(10) (= 10^{-3}M). (d_6-DMSO)

Solution emission behaviour of CN-PLLA(21) and (145)

Solution emission responses toward concentration and aggregation are used to characterize the AEE property of CN-PLLA(21) and (145). The concentration effect is emphasized by the non-normalized solution emission spectra in Figure 3, which show the same emission behaviour for both solutions that the emission intensity increases with increasing concentration from 10^{-6} to 10^{-3} M (relative to the molar content of the fluorescent CN center in THF). The concentration-enhanced emission observed here is correlated with the AEE effect.

Primary comparison on the high and low MW CN-PLLA(145) and (21) can be made here. Since the solution emission spectra are recorded in solutions with constant CN content, solutions of CN-PLLA(21) and (145) should emit with the same intensity if no other external factor was involved. Although the observed difference in Figure 3 is minor, we still can identify that solutions of the high MW CN-PLLA(145) always emit with higher intensity compared to the low MW CN-PLLA(21). The intensity difference observed here indicates that the PLLA chains indeed affect the emission of CN unit, that is, the high MW PLLA chains of CN-PLLA(145) exert more viscous dragging forces and therefore, imposing more rotational restriction on the neighbouring CN center than the low MW PLLA chains of CN-PLLA(21). Thus, effective rotational restriction imposed by the high MW PLLA chains of CN-PLLA(145) result in emission with higher intensity than the less-effective rotation blocker of the low MW PLLA chains of CN-PLLA(21). The result is correlated with RIR mechanism generally involved in AIE- and AEE-active fluorophores, however, the present system is rare in considering that the structural unit responsible for the varied rotational restriction and AEE-related emission efficiency is the neighbouring PLLA chains rather than the fluorescent CN center itself.

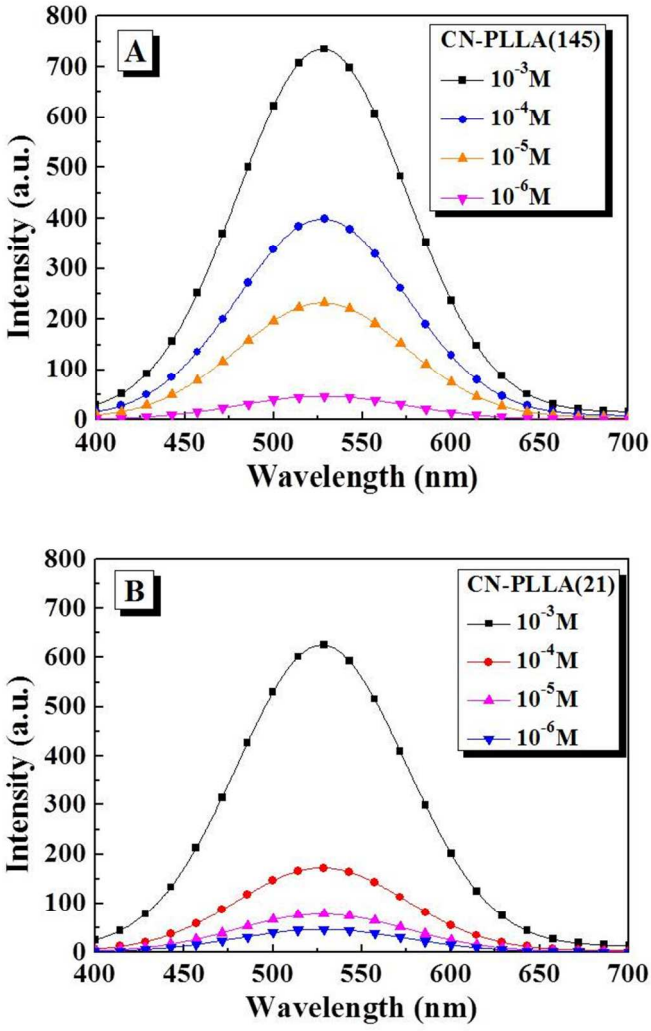

Figure 3 Solution emission spectra of (A) CN-PLLA(145) and (B) CN-PLLA(21) in THF at various concentrations from 10^{-6} to 10^{-3} M (excited at 365 nm).

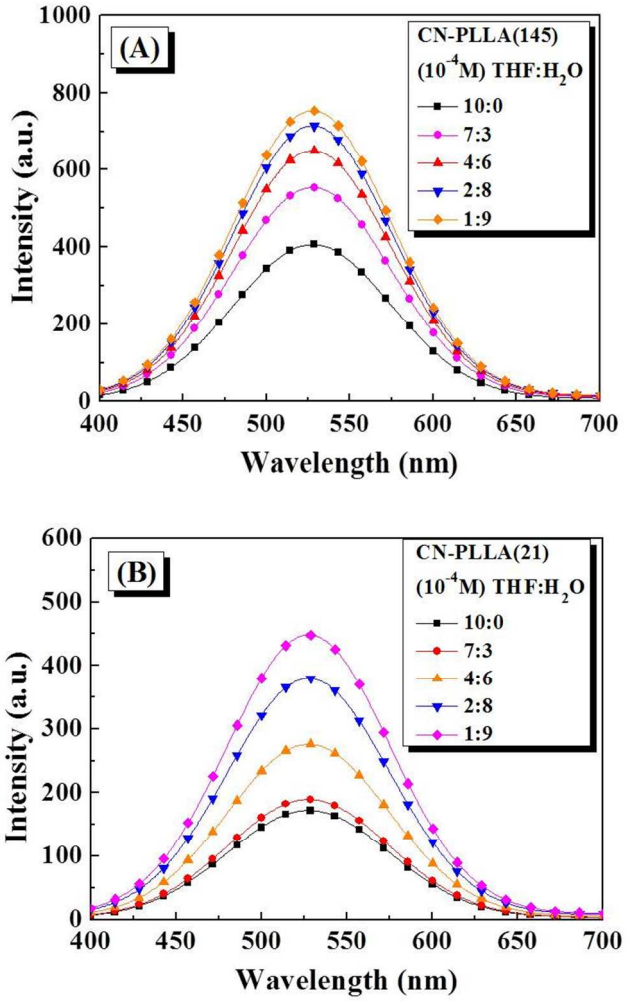

Figure 4 Solution emission spectra of (A) CN-PLLA(145) and (B) CN-PLLA(21) in THF/water solvent mixtures containing different amounts of water. (λ_{ex} = 365 nm).

The AEE property can be also evaluated from the emission response toward aggregation. By adding different amounts of nonsolvent water to the pure THF solution of CN-PLLA(n), aggregated CN-PPLA(n) solutions can be generated for emission measurements. The emission spectra of CN-PLLA(n)s in THF/water mixtures (Figure 4) exhibit the general trend that the solution emission increases with increasing water content in the solution. By keeping concentration of the CN unit at a constant value of 10-4 M, the emission intensity of the CN-PLLA(n) solutions can be raised by increasing water content in the solutions. As correlated with the emission spectra in Figure 3, the high MW CN-PLLA(145) solution also emits with higher intensity than the low MW CN-PLLA(21). Within the aggregated particles formed in the solution mixtures, the CN center connected by high MW PLLA chains is supposed to be more sluggish in rotation than the CN center in the low MW PLLA chains.

Formation of aggregated particles in the solution mixtures can be confirmed form the DLS analysis. As illustrated in Figure 5, the aggregated nanoparticles formed in both solutions became smaller when more water was added into the pure THF solutions of CN-PLLA(n)s. The shrunk aggregates formed in solutions of higher water content are therefore responsible for the emission enhancement observed in Figure 4. Free molecular rotation of the fluorescent CN unit is supposed to be more effectively confined when it is situated in limited spaces of shrunk nanoparticles, regarding to the steric constraints imposed by the congested environment. The sluggish molecular rotations in the confined space of shrunk nanoparticles promote the AEE-related emission by blocking the non-radiative decay pathways coupled with molecular motion. Although higher in the chain dimension, high MW CN-PLLA(145) actually exhibit more drastic size reduction than the low MW CN-PLLA(21). When the water content was increased from 30 to 70 vol%, the average hydrodynamic diameters of the CN-PLLA(21) particles decrease from 300 to 210 nm, such a size change is smaller in magnitude than the high MW CN-PLLA(145) (size decreases from 530 to 140 nm). Supposedly, the low solubility of the high MW CN-PLLA(145) in water is responsible for the large variation of the particle size.

Crystallization-promoted emission enhancement of the solid CN-PLLA(n)s

Primarily, solid CN-PLLA(n)s were subjected to DSC scan to reveal the possible conformational change upon thermal treatment. The first DSC scans (Figure 6A) of CN-PLLA(145) and (21) results in the single melting transition (T_m) at 160 and 146 ^oC, respectively. With a higher T_m, CN-PLLA(145) should contain more perfect crystals than the low MW CN-PLLA(21) with lower T_m. MW difference also contributes to the different levels of crystallinity, which will be discussed later.

The 2nd DSC runs (Figure 6B), after cooling from the respective molten states, of both samples result in thermograms consisting of glass transition, recrystallization exotherm and T_m at temperature lower than the first-scan. Here, the newly-formed glass transition is attributed to amorphous chains generated from melting during the first DSC scan, but the subsequent recrystallization results in crystals of less perfection, which was subsequently melt at a T_m comparatively lower than the first DSC run of the as-synthesized CN-PLLA(n)s. The DSC thermograms presented here indicates the possibility of generating amorphous CN-PPLA(n)s by thermal treatment.

Previous study[42] suggests that emission of pure CN4OH is strongly correlated with the CEE property, experimental procedures (e.g. solvent-fuming) leading to increasing crystallinity also enhance the emission of CN4OH. CEE is nevertheless irrelevant to the present case in considering the molecular architecture of the CN-PPLA(n)s. Single polymer chain of CN-PLLA(n)s contain only one CN fluorophore and large-scale, crystalline CN domains are difficult to form since all the fluorescent CN units in CN-PLLA(n)s are essentially isolated from each other by the surrounding lactide polymer chains. Instead of the fluorescent CN center, crystallization of the neighbouring PLLA chains should be the main factor of controlling the emission behaviour of CN-PLLA(n)s. As crystallinity of polylactides46 is indeed affected by the MW difference, CN-PLLA(21) and (145) of low and high MWs were prepared and characterized to clarify the role of lactide's crystallinity on the AEE activity of the CN center.

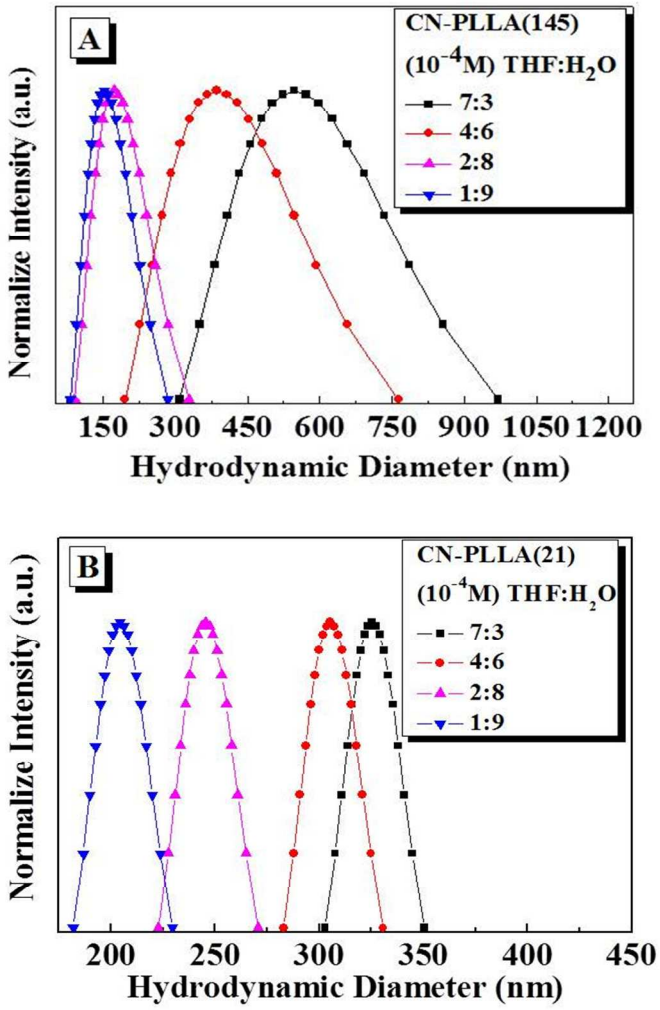

Figure 5 histograms of hydrodynamic diameters of (A) CN-PLLA(145) and (B) CN-PLLA(21) in THF/water solvent mixtures containing different amounts of water.

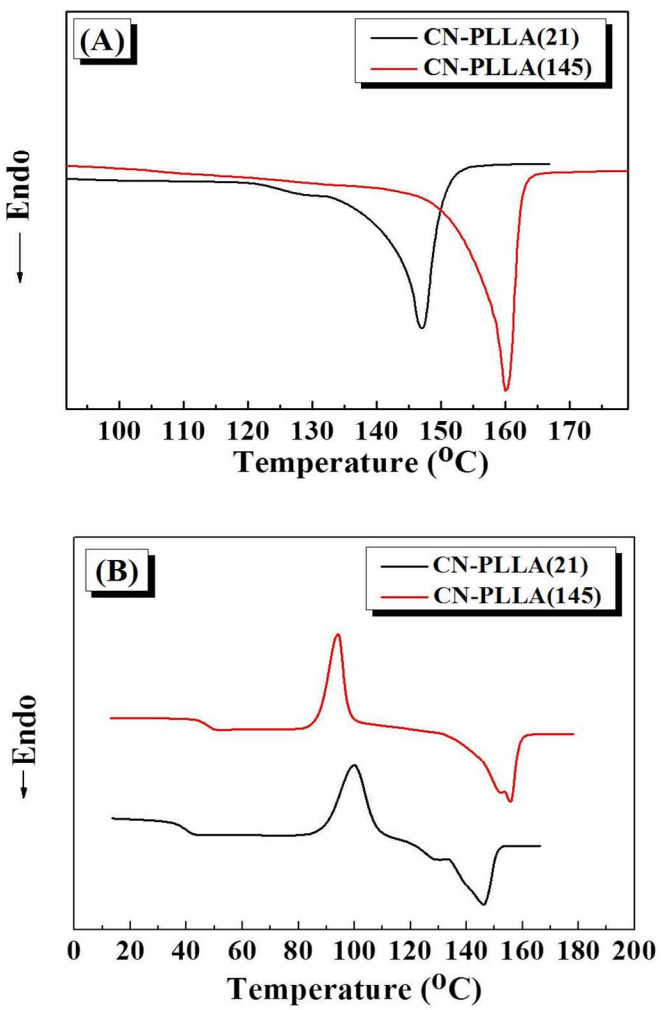

Figure 6 DSC traces of CN-PLLA(145) and CN-PLLA(21) in (A) the first heating run and (B) the second heating runs. (heating rate = 10 ^{o}C/min)

The emission spectra of the as-synthesized crystalline solids in Figure 7 indicate that the emission intensity of the high MW CN-PLLA(145) is higher than the small MW CN-PLLA(21). Solution emission spectra in Figure 3 and 4 also show the same intensity profile but the cause may be different since the fluorescent CN contents of the solid CN-PLLA(n)s are not the same as they are in the solution emission measurements. For the solid CN-PLLA(n)s, the polymeric PLLA chains function as diluent to lower the content of the fluorescent CNs. The high MW PLLA chain of CN-PLLA(145) acts to dilute the CN content to a value lower than the CN content of CN-PLLA(21). Despite lower in the fluorescent CN content, CN-PLLA(145) is however a stronger emitter compared to CN-PLLA(21) with higher CN content. More realistic data can be adopted from the quantum yield (ΦF) data measured from the integration sphere. The resulting ΦFs of CN-PLLA(n)s are also compared with pure CN4OH in Table 1. The result indicates that the emission efficiencies of all three solids are in the order of CN-PLLA(145) > CN-PLLA(21) > CN4OH, that is, the one with lower fluorescent content happens to be higher in the resolved Φ_F value. Clearly, effective rotational restriction on the AEE-active fluorophores plays more decisive role than the fluorescent content.

The crucial role of lactide's crystallinity on the emission of CN-PLLA(n)s can be best demonstrated by comparing the emission intensity between the amorphous and the crystalline samples. The amorphous polymers can be easily obtained by quickly quenching the molten samples into the liquid nitrogen. The emission spectra of the amorphous CN-PLLA(n)s were therefore measured and compared with the crystalline samples in Figure 7. As anticipated, the crystalline CN-PLLA(21) and (145) are all much higher in emission intensity than their respective amorphous samples. For both CN-PLLA(145) and (21), the emission intensities of the crystalline samples are at least ten times to those of the amorphous solids; therefore, crystallinity of the PLLA chains is crucial for the emission of the central CN unit. Nature of the amorphous and the crystalline chains can be separately identified by the WAXD spectra.

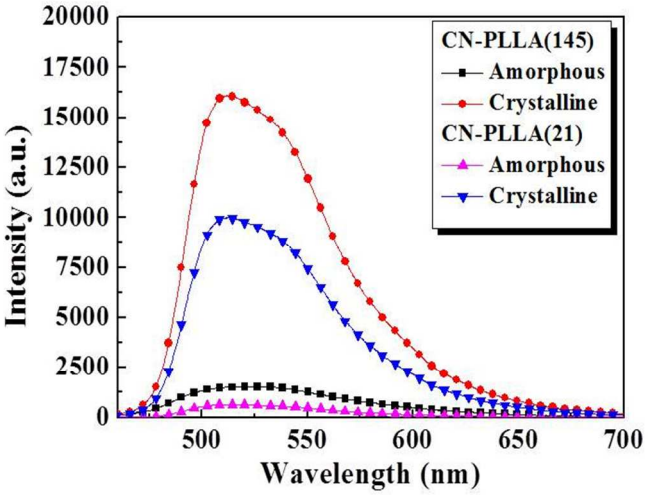

Figure 7 Solid emission spectra of amorphous and crystalline of CN-PLLA(145) and CN-PLLA(21).

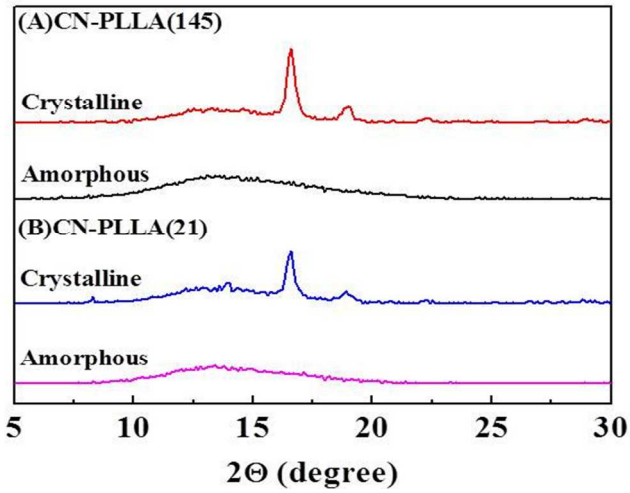

Figure 8 WAXD spectra of amorphous and crystalline of (A) CN-PLLA(145) and (B) CN-PLLA(21)

Table 2 Quantum yield (Φ_F)[a] and crystallinity[b] of the solid CN-PLLA(145), CN-PLLA(21) and CN4OH.

sample	CN-PLLA(145)	CN-PLLA(21)	CN4OH
Φ_F(%)	31	22	15
Crystallinity (%)	57	48	38

[a]determined from integrating sphere. [b]determined from the deconvoluted WAXD spectra (Figure S13, supporting information) as the ratio of the integrated diffraction intensity of the crystalline peak to the whole scattering.

As illustrated in Figure 8, the samples quenched from the molten states are no doubt amorphous in view that the spectra mainly consist of broad diffraction halos, which is widely different from the resolved diffraction peaks for the crystalline CN-PLLA(n)s. The spectra of the crystalline CN-PLLA(n)s consist of two strong diffraction peaks at 2θ = 16.7 and 19.1 o, which are characteristic diffractions for the α-helical crystal of polylactides.29 Comparatively, the high MW CN-PLLA(145) are higher in crystallinity than the low MW CN-PLLA(21) as indicated by the resulting crystallinity (57 vs. 48%, Table 2) calculated from the WAXD spectra. Crystallinity of the PLLA chains is therefore the key factor of controlling emission efficiency of CN-PLLA(145) and (21). The crystalline PLLA chains are efficient in imposing effective rotational restriction on the neighbouring CN center in considering that crystalline lattices contain less molecular voids and defects. The fluorescent CNs embedded in crystalline PLLA lattices are therefore more efficient in emission compared to fluorescent CNs in the amorphous regions. With higher fraction of crystalline chains, crystalline CN-PLLA(145) therefore emits with higher intensity than CN-PLLA(21) containing less crystalline PLLA chains

Previously, there are examples[22,47] illustrating the use of solvent-fuming in raising the crystallinity and the concurrent emission efficiency of the CEE-active fluorophores. Solvent-fuming was therefore used in this study; however, instead of raising the crystallinity of the fluorophores, solvent-fuming employed here is used for increasing crystallinity of the non-luminescent PLLA chains. With this respect, the amorphous CN-PLLA(n)s from the quenched molten state were placed in close vessels saturated with ethanol vapor for different time periods before withdrawn for spectral measurement. As illustrated in Figure 9, emission intensity of CN-PLLA(145) was gradually enhanced with increasing exposure time under ethanol vapour, and the maximum emission intensity of the fumed film, after 25 min of exposure, is more than 3.7 times to the initial intensity of the amorphous film before fuming. The emission enhancement of the amorphous CN-PLLA(21) is even more drastic, for which we observe a 5.3-fold intensity enhancement after 25 min of exposure time. The high sensitivity of CN-PLLA(21) is attributed to the high mobility of the low MW PLLA chains. Corresponding WAXD spectra (Figure S15) indicate that solvent-fuming process indeed transforms the amorphous samples into the crystalline materials with the observed diffraction peaks located at the same positions as Figure 8.

Possible causes leading to the observed CPEE phenomenon can be qualitatively illustrated by Scheme 2, which gives the chain conformation difference between the amorphous and the crystalline CN-PLLA(n)s. The PLLA chains of the amorphous CN-PLLA samples presumably adopt the flexible, random chain conformation. Conceptually, the random PLLA chains developed from the CN center should provide efficient steric bulkiness to shield the CN center from contact of the other CN units. The CN centers in the amorphous CN-PLLA(n)s are thus isolated from each other by the randomly-distributed PLLA chains in the neighbourhood and intermolecular aggregation of the CN centers buried in the amorphous lactide chains is rather difficult. Therefore, the corresponding emissions of the amorphous CN-PLLA(n)s are very weak (cf. Figure 7) due to the difficulty in forming aggregates of CN units.

For crystalline CN-PLLA(n)s, intermolecular aggregation of the CN centers is highly probable in view of the short intermolecular distance of the CN centers in the intimately-

packed PLLA chains. The α-form polylactide crystal possesses an orthorhombic unit-cell[29] of parameters a = 1.06 nm, b = 0.61 nm and c = 2.88 nm. The lattice parameters evaluated from the WAXD spectra (Figure 8) are in the close vicinities of the reported values, with a = 1.07, b = 0.62 and c = 2.92 nm for CN-PLLA(145) and a = 1.07 nm, b = 0.62 nm and c = 2.87 nm for CN-PLLA(21). Accordingly, the neighbouring helical chains are in closely-packed fashion with the nearest inter-chain distance of 0.61 nm as calculated from the parameters. A helical packing with such short inter-chain distance is different from the previous reported polypeptide of TP-2PBLG.[48] Similar to CN-PLLA(n)s, TP-2PBLG possesses a chemical structure that the AIE-active tetraphenylthiophene (TP) center is chemically linked with two peptide chains of poly(γ-benzyl-L-glutamate) (PBLG). With a similar chemical structure, TP-2PBLG however is a poor emitter with weak emission in the solution and in the solid film states. Weak emission of TP-2PBLG is attributed to the dimension difference between the α-helical peptide chain and the TP center. Intermolecular aggregation of the TP (with a molecular width of 0.9 nm) centers is effectively blocked by the large α-helical peptide chains of PBLG in the diameter range from 1.5 to 2.5 nm.[25,48-51]

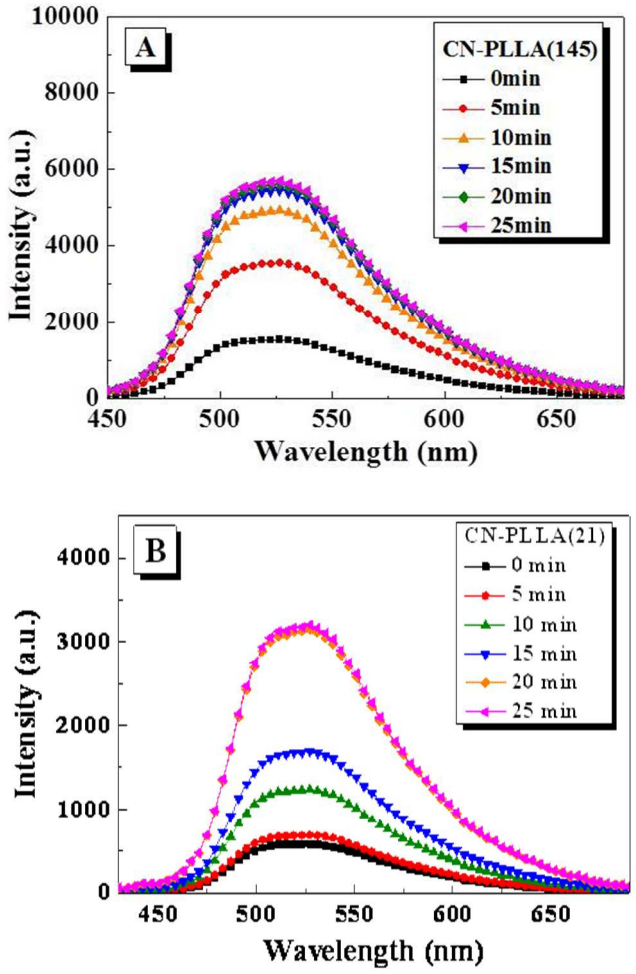

Figure 9 Changes of (A) CN-PLLA(145) and (B) CN-PLLA(21) in the emission intensity with the exposure time to ethanol vapor. (λ_{ex} = 365 nm).

In contrast, No such aggregation difficulty exist in CN-PLLA(n)s since the resolved inter-chain distance of 0.61 nm is small enough for a close contact of the inherent CN centers. The CN centers held by the close-packed PLLA chains are supposed to be clumsy in rotation in considering the limited free voids and defects in the intimately-packed orthorhombic lattices. Rotational restriction imposed by the neighbouring PLLA chains is therefore the decisive mechanism responsible for the emission of the crystalline CN-PLLA(n)s. In contrast, the intimately-packed CN centers are nevertheless absent in the amorphous CN-PLLA(n)s. Once ruptured by thermal forces, the crystalline PLLA chains start to redistribute and mobilize to form random chain segments around the CN centers; at this stage, the PLLA chains behave as steric blocker to efficiently shield the CN centers from approaching each other, forming aggregates of appreciable sizes. Failure in forming CN aggregates in close vicinities is therefore responsible for the weak emissions of the amorphous CN-PLLA(n)s. The amorphous PLLA chains in random chain conformation is considered to be detrimental to the aggregation and the accompanied AEE-related emission of CN-PLLA(n)s.

Conclusion

We prepared CN-PLLA(n) polymers by ROP initiated by the *p*-OH groups of CN4OH. The ^{1}H NMR spectra of all related molecules successfully demonstrate that the *p*-OH groups are essentially the initiating sites to induce ROP of the lactide monomer, generating highly-emissive CN-PLLA(n)s with the preserved *o*-OH groups to maintain the rigid enolimine rings.

In the solution state, the longer PLLA chain of the high MW CN-PLLA(145) exerts strong viscous dragging forces and therefore imposes more effective rotational restriction on the central CN, thus, rendering in solution emission with higher intensity than the low MW CN-PLLA(21) with shorter PLLA chain. For the solid sample, raising MW of PLLA chains increases the crystallinity of the neighbouring PLLA chains, resulting in solid emission with intensity than the low MW CN-PLLA(21). With lower fluorescent CN content, CN-PLLA(145) is however higher in emission efficiency than the CN-PLLA(21) containing higher fluorescent unit; therefore, effective rotational restriction, rather than the fluorophore content, imposed by the crystalline PLLA chains is the key factor of controlling the emission efficiency of the crystalline CN-PLLA(n)s. Crystalline CN-PLLA(n)s are therefore much better emitters than the amorphous CN-PLLA(n)s. Held by intimately-packed PLLA chains, the CN centers can approach each other to form aggregated species with hampered rotation, resulting in emission with intensity than the amorphous CN-PLLA(n) containing randomized PLLA chains. CPEE property induced by the neighbouring crystalline PLLA chains is therefore identified in this study.

Acknowledgements

We appreciate the financial support from National Science Council, Taiwan, under the contract no. NSC 102-2221-E-110-084-MY3.

References

(1) Luo, J.; Xie, Z.; Lam, J. W. Y.; Cheng, L.; Chen, H.; Qiu, C.; Kwok, H. S.; Zhan, X.; Liu, Y.; Zhu, D.; Tang, B. Z. Chem. Commun. 2001, 1740–1741.

(2) Tang, B. Z.; Zhan, X.; Yu, G.; Lee, P. P. S.; Liu, Y.; Zhu, D. J. Mater. Chem., 2001, 11, 2974−2981.

(3) Hong, Y.; Lam, J. W. Y.; Tang, B. Z. Chem. Commun. 2009, 29, 4332–4353.

(4) Ding, D.; Li, K.; Liu, B.; Tang, B. Z. Acc. Chem. Res. 2013, 46, 2441–2453.

(5) Zhao, Z.; Lam, J. W. Y.; Tang, B. Z. J. Mater. Chem. 2012, 22, 23726–23740.

(6) Wang, M.; Zhang, G.; Zhang, D.; Zhu, D.; Tang, B. Z. J. Mater. Chem. 2010, 20, 1858–1867.

(7) Zhao, Z.; Lam, J. W. Y.; Tang, B. Z. Soft Matter 2013, 9, 4564–4579.

(8) Aggregation-Induced Emission: Fundamentals, ed. Qin, A. and Tang, B. Z.; John Wiley & Sons, Ltd, N. Y., 2013.

(9) Birks, J. B.; Photophysics of Aromatic Molecules, Wiley, London, 1970.

(10) Hong, Y.; Lam, J. W. Y.; Tang, B. Z. Chem. Soc. Rev. 2011, 40, 5361–5388.

(11) Hu, R.; Leung, N. L. C.; Tang, B. Z. Chem. Soc. Rev. 2014, 43, 4494–4562.

(12) Zhang, G. F.; Aldred, M. P.; Gong, W. L.; Li, C.; Zhu, M. Q. Chem. Commun. 2012, 48, 7711–7713

(13) Shuang, Z.; Qin, A.; Sun, J. Z.; Tang, B. Z. Prog. Chem. 2011, 23, 623–636.

(14) Mei, J.; Hong, Y.; Lam, J. W. Y.; Qin, A,; Tang, Y.; Tang, B. Z. Adv. Mater. 2014, 26, 5429–5479.

(15) Li, Z.; Dong, Y.; Mi, B.; Tang, Y.; Häussler, M.; Tong, H.; Dong, Y.; Lam, J. W. Y.; Ren, Y.; Sung, H. H. Y.; Wong, K. S.; Gao, P.; Williams, I. D.; Kwok, H. S.; Tang, B. Z. J. Phys. Chem. B 2005, 109, 10061–10066.

(16) Chen, J.; Law, C. C. W.; Lam, J. W. Y.; Dong, Y.; Lo, S. M. F.; Williams, I. D.; Zhu, D.; Tang, B. Z. Chem. Mater. 2003, 15, 1535–1546.

(17) Dong, Y.; Lam, J. W. Y.; Qin, A.; Sun, J.; Liu, J.; Li, Z.; Sun, J.; Sung, H. H. Y.; Williams, I. D.; Kwok, H. S.; Tang, B. Z. Chem. Commun. 2007, 3255–3257.

(18) Dong, Y.; Lam, J. W. Y.; Qin, A.; Liu, J.; Li, Z.; Tang, B. Z.; Sun, J.; Kwok, H. S. Appl. Phys. Lett. 2007, 91, 011111.

(19) Tong, H.; Dong, Y.; Häussler, H.; Lam, J. W. Y.; Sung, H. H. Y.; Williams, I. D.; Sun, J.; Tang, B. Z. Chem. Commun. 2006, 1133–1135.

(20) Dong, Y.; Lam, J. W. Y.; Qin, A.; Li, Z.; Sun, J.; Sung, H. H. Y.; Williams, I. D.; Tang, B. Z. Chem. Commun. 2007, 40–42.

(21) Tong, H.; Dong, Y.; Hong, Y.; Häussler, H.; Lam, J. W. Y.; Sung, H. H. Y.; Yu, X.; Sun, J.; Williams, I. D.; Kwok, H. S.; Tang, B. Z. J. Phys. Chem. C 2007, 111, 2287–2294.

(22) Qian, L.; Tong, B.; Shen, J.; Shi, J.; Zhi, J.; Dong, Y.; Yang, F.; Dong, Y.; Lam, J. W. Y.; Liu, Y.; Tang, B. Z. J. Phys. Chem. B 2009, 113, 9098–9103.

(23) Chien, W. L.; Yang, C. M.; Chen, T. L.; Li, S. T.; Hong, J. L. RSC Adv. 2013, 3, 6930–6938.

(24) Ikada, Y.; Tsuji, H. Macromol. Rapid Commun. 2000, 21, 117–132.

(25) De Santis, P.; Kovacs, P. J. Biopolymers 1968, 6, 299–306.

(26) Zhang, J.; Duan, Y.; Sato, H.; Tsuji, H.; Noda, I.; Yan, S.; Ozaki, Y. Macromolecules 2005, 38, 8012–8021.

(27) Kalb, B.; Pennings, A. J. Polymer 1980, 21, 607–612.

(28) Puiggali, J.; Ikada, Y.; Tsuji, H.; Cartier, L.; Okinara, T.; Lotz, B. Polymer 2000, 41, 8921–8930.

(29) Cartier, L.; Okihara, T.; Ikada, Y.; Tsuji, H.; Puiggali, J.; Lotz, B. Polymer 2000, 41, 8909–8919.

(30) Hoogsteen, W.; Postema, A. R.; Pennings, A. J.; ten Brinke, G.; Zugenmaier, P. Macromolecules, 1990, 23, 634–642.

(31) Zhang, J.; Tashiro, K.; Tsuji, H.; Domb, A. J. Macromolecules 2008, 41, 1352–1357.

(32) Li, Y.; Hana, C.; Bian, Y.; Dong, Q.; Zhao, H.; Zhang, X.; Xu, M.; Don, L. Thermochimica Acta 2014, 580, 53–62.

(33) Drumright, R. E.; Grubber, P. R.; Henton, D. E. Adv. Mater. 2000, 12, 1841–1846.

(34) Tang, X.; Xiang, Y.; Tong, A. J. J. Org. Chem. 2009, 74, 2163–2166.

(35) Berezin, M. Y.; Achilefu, S. Chem. Rev. 2010, 110, 2641–2684.

(36) Hsieh, C. C.; Cheng, Y. M.; Hsu, C. J.; Chen, K. Y.; Chou, P. T. J. Phys. Chem. A 2008, 112, 8323–8332.

(37) Henary, M. M.; Fahrni, C. J. J. Phys. Chem. A 2002, 106, 5210–5220.

(38) Mordzinski, A. Grabowska, A. Chem. Phys. Lett. 1982, 90, 122–127.

(39) Douhal, A.; Lahmani, F.; Zewail, A. H. Chem. Phys. 1996, 207, 477–498.

(40) Lochbrunner, S.; Schultz, T.; Schmitt, M.; Shaffer, J. P.; Zgierski, M. Z.; Stolow, A. J. Chem. Phys. 2001, 114, 2519–2522.

(41) Goodman, J.; Brus, L. E. J. Am. Chem. Soc. 1978, 100, 7472–7474.

(42) Deng, S. L.; Chen, T. L.; Chien, W. L.; Hong, J. L. J. Mater. Chem. C 2014, 2, 651–659.

(43) Stirey, R. F.; Sherman, J. W. Macromolecules 2002, 35, 1504–1512.

(44) Lai, C. T.; Chien, R. H.; Kuo, S. W.; Hong, J. L. Macromolecules 2011, 44, 6546–6556.

(45) Chien, R. H.; Lai, C. T.; Hong, J. L. J. Phys. Chem. C 2011, 115, 20732– 20739.

(46) Tsuji, H.; Ikada, Y. Polymer 1999, 40, 6699–6708.

(47) Yang, C. M.; Lee, I. W.; Chen, T. L.; Chien, W. L.; Hong, J. L. J. Mater. Chem. C 2013, 1, 2842–2850.

(48) S. T. Li, Y. C. Lin, W. T. Chuang, S. W. Kuo and J. L. Hong, Polym. Chem., 2012, 3, 2393–2402.

(49) T. Torii, T. Yamashita and K. Horie, Eur. Polym. J., 1993, 29, 1265–1270.

(50) P. Doty, J. H. Bradbury, and A. M. Holtzer, J. Am. Chem. Soc., 1956, 78, 947–954.

(51) F. A. Bovey, and G. V. D. Tiers, Adv. Polym. Sci., 1963, 3, 139–195.

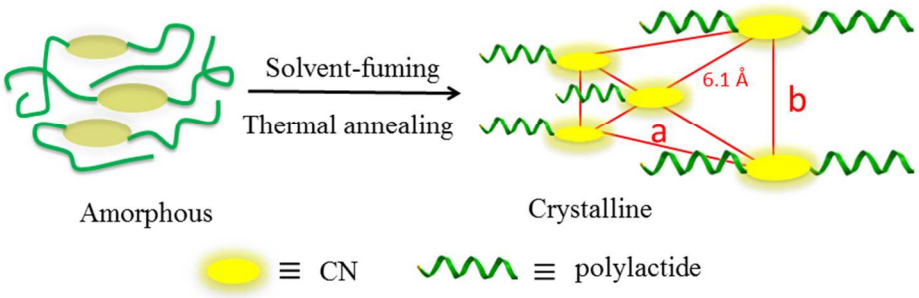

254x190mm (96 x 96 DPI)